ELSEVIER

Chemical Engineering Journal 118 (2006) 1–10

Chemical Engineering Journal

www.elsevier.com/locate/cej

Numerical prediction of combustion of carbon particle clusters in a circulating fluidized bed riser

Zhao Yunhau [a], Lu Huilin [a,*], He Yurong [a], Jianmin Ding [b], Yin Lijie [a]

[a] *School of Energy Science and Engineering, Harbin Institute of Technology, Harbin 150001, China*
[b] *MSC Software, 2 MacArthur Place, Santa Ana, CA 92707, USA*

Received 2 August 2005; received in revised form 2 December 2005; accepted 30 December 2005

Abstract

The burning properties of carbon particles in clusters were numerically studied using a mathematical model. Chemical reactions consist in heterogeneous reactions including char combustion and in gases homogeneous reactions. The numerical model predicted gas flux through a cluster, distributions of gas temperature and concentrations of gas species in clusters. Burnout of char particles in cluster is less than that of isolated char particles in the stream. Formation of NO and N_2O are restrained from particle clustering. Effects of inlet gas temperature, inlet gas velocity, distribution of particles in cluster as well as particle size on char combustion and flow behavior are numerically investigated.

Keywords: Cluster; Char combustion; Numerical simulation; Circulating fluidized bed riser

1. Introduction

Circulating fluidized bed (CFB) combustion technology has grown in importance in last two decades as boiler manufacturers and users have recognized the advantages of this technology, such as outstanding fuel flexibility, low emission of pollutants and adaptability to load change [1–4]. It is generally agreed that in a circulating fluidized bed boiler, the suspension partly condenses into denser clusters that move upwards through the center of furnace. At some point, they get swept towards the low velocity region near the wall, where clusters reverse their flow direction and falling along the wall [5]. Experiments have shown cluster flow characterization [6] and measured cluster formation frequency, cluster distributions [7–14] as well as contact time between cluster and wall [14]. Results from these experiments suggest that clusters play an important role on performance of a circulating fluidized bed reactor. Hence, detailed knowledge of contributions of particle clusters to combustion in the circulating fluidized beds is necessary. Some researchers have incorporated the concept of particle clusters into hydrodynamic models of circulating fluidized beds leading to promising predictions of experimental results [15–19]. Computed results found that air flow through clusters can be negligible for porosity in the cluster range from 70 to 90% [19].

Based on model of single coal particle combustion, many numerical simulations have been performed to obtain combustion behavior of coal particles in circulating fluidized bed combustors. Softdeh-Gharebeagh et al. [20] developed a coal combustion model via ASPEN tool to predict the CFB combustion efficiency and emission levels in CFBs. The effect of operating conditions on carbon combustion efficiency and sulphur retention was investigated in circulating fluidized bed combustors [21–23]. Myohanen et al. [24] presented a three-dimensional, steady state combustion model for predicting heat flux profile in a large-scale supercritical circulating fluidized bed boiler. Knoebig et al. [25] developed a circulating fluidized bed combustion model to investigate effect of gas–particles mixture on emission in a large-scale circulating fluidized bed boiler furnace.

Present study is to focus on effects of carbon particle clusters on reaction in a CFB reactor riser. Combustion behavior of carbon particle in clusters was numerically simulated. Chemical reactions modeled including heterogeneous reactions of char cluster reacting with surrounding O_2, CO, CO_2, NO, and N_2O, and homogeneous reactions of among CO, O_2, NO, and N_2O. The clusters were assumed steady in the riser while gases flow

* Corresponding author.
E-mail address: huilin@hit.edu.cn (L. Huilin).

1385-8947/$ – see front matter © 2006 Elsevier B.V. All rights reserved.
doi:10.1016/j.cej.2005.12.023

Nomenclature

c_g	specific heat (kJ/kg K)
C_1, C_2	empirically determined constants
[CO]	concentration of carbon monoxide (mol/m^3)
d_p	particle diameter (μm)
D	molecular diffusion coefficient (m^2/s)
E	activation energy (J/mol)
[H_2O]	moisture concentration (kmol/m^3)
i, j, k	coordinate directions
k	gas phase turbulent kinetic energy (m^2/s^2)
k_i	reaction rates (kmol/m^3 s)
m_p	mass of single particle (kg)
$\dot{m}$	rate of change of mass (kg/s)
n_r	cell number along r direction
n_x	cell number along x direction
[NO]	concentration of nitrous monoxide (%)
[N_2O]	nitrous oxide concentration (%)
[O_2]	oxygen concentration (kmol/m^3)
p	partial pressure (kPa)
Q	heat source (kJ/kg)
r	radial direction (m)
r_k	rate of production of species k (kg/m^3 s)
R_c	radius of cluster (μm)
R_A, R_B, …, R_k	reaction rate (mol/m^3 s)
T	temperature (K)
u	gas velocity (m/s)
u_g	inlet gas velocity (m/s)
V	gas flux (m^3/s)
V_{total}	total gas flux through sectional area of cluster (m^3/s)
x	vertical coordinate (m)
Y_i	mass fraction of species i

Greek letters

α	primary CO/CO_2 product ratio
ε	energy dissipation rate (m^2/s^3)
λ	effective thermal conductivity (W/m °C)
μ	viscosity (kg/m s)
ν	gas phase kinematic viscosity (m^2/s)
ρ	density (kg/m^3)
σ	empirically determined constant

Subscripts

C	carbon
g	gas phase
R	at particle surface
s	solid phase

through the clusters. Numerical results showed distributions of gas temperature and gas species in the cluster. It is found that the carbon burnout of particles in the cluster was much less than that of an isolated char particle in the reacting stream. Effects of temperature and inlet flow rate on thermal characteristics and chemical reaction kinetics was also investigated.

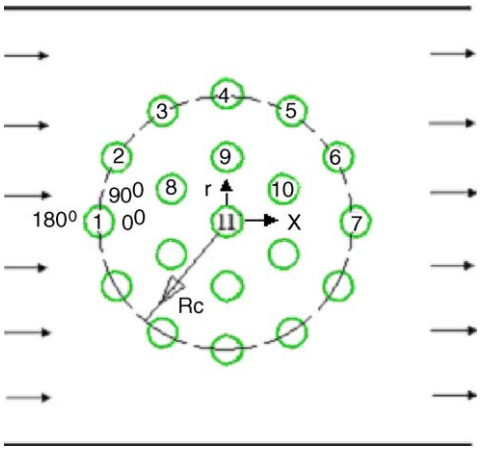

Fig. 1. Configuration of base case cluster.

2. Governing equations

Fig. 1 shows the geometry of the cluster. A cluster is modeled as a round two-dimensional disk distributed in the riser. The radius of the cluster disk is R_c. We assumed that: (1) particles are uniformly distributed in space, and remain quiescent. (2) Particle diameter was assumed to be constant in combustion. The spherical shape of a particle is assumed and remained constant during combustion. (3) Radiation heat transfer between gas and particle are neglected due to small different temperature between them. For simplicity, radiation heat transfer between particle and the walls are not accounted in present study. From these assumptions, the conservation equations of mass, species and energy in Eulerian coordinates are given as follows.

2.1. Gas phase continuity equation

The steady state mass conservation equation of gas can be written as follows [26,27]:

$$\frac{\partial}{\partial x_j}(\rho u_j) = -\sum_k n_k \dot{m}_k \tag{1}$$

The term at right-hand side of Eq. (1) expresses mass source from char particle combustion.

2.2. Gas phase momentum equation

The conservation of momentum for gas phase is expressed as follows [26,27]:

$$\frac{\partial}{\partial x_j}(\rho u_j u_i) = \frac{\partial p}{\partial x_i} + \frac{\partial}{\partial x_j}\left(\mu_g \frac{\partial u_j}{\partial x_i}\right) + \frac{\partial}{\partial x_j}\left(\mu_g \frac{\partial u_i}{\partial x_j}\right) + \rho_g g - u_i \sum_k n_k \dot{m}_k \tag{2}$$

The last term at right-hand side of Eq. (2) accounts for source from char particle combustion.

2.3. Turbulence model for gas phase

In present study, we employ the standard k–ε turbulence model for simulating turbulent flow in the riser [27]. The standard k–ε turbulence model gives gas phase equations of turbulent kinetic energy:

$$\frac{\partial}{\partial x_j}(\rho u_j k) = \frac{\partial}{\partial x_j}\left(\frac{\mu_g}{\sigma_k}\frac{\partial k}{\partial x_j}\right) + G_k - \rho_g \varepsilon + G_R \quad (3)$$

and turbulent kinetic energy dissipation rate:

$$\frac{\partial}{\partial x_j}(\rho_g u_j \varepsilon) = \frac{\partial}{\partial x_j}\left(\frac{\mu_g}{\sigma_\varepsilon}\frac{\partial \varepsilon}{\partial x_j}\right) + \frac{\varepsilon}{k}[C_1 G_k - C_2 \rho_g \varepsilon] + \frac{\varepsilon}{k} C_1 G_R \quad (4)$$

where G_k is the production term.

$$G_k = \mu_g\left(\frac{\partial u_i}{\partial x_j} + \frac{\partial u_j}{\partial x_i}\right)\frac{\partial u_i}{\partial x_j} - \frac{2}{3}\delta_{ij}\frac{\partial u_k}{\partial x_k} \quad (5)$$

where $\mu_g = \mu_l + \mu_t$ is the effective viscosity, $\mu_t = C_\mu \rho_g k^2/\varepsilon$ the gas phase turbulent viscosity, and $G_R = -k\sum_k n_k \dot{m}_k$ is the production term from char particle combustion. The empirical constants, C_μ, σ_ε, C_1 and C_2, are listed in Table 2.

2.4. Energy conservation of gas phase

The energy balance equation of gas phase is written as follows [26]:

$$\frac{\partial}{\partial x_j}(\rho_g u_j C_g T_g) = \frac{\partial}{\partial x_j}\left[\left(\lambda_g + \frac{\mu_\varepsilon}{\sigma_h}\right)\frac{\partial}{\partial x_j}(C_g T_g)\right] + Q_s \quad (6)$$

where Q_s is the heat sources per unit volume, including convective heat transfer between particle and gas and heat release of reactions. As in previous assumption, radiation heat transfer process is not accounted in Eq. (6).

2.5. Species conservation equation of gas phase

The mass balance for a gas species k ($k = CO_2$, CO, O_2, NO, and N_2O) is [26,27]:

$$\frac{\partial}{\partial x_j}(\rho_g u_j Y_k) = \frac{\partial}{\partial x_j}\left(D_k + \frac{\mu_g}{\sigma}\frac{\partial Y_k}{\partial x_j}\right) + \sum_{k=1}^{5} R_k \quad (7)$$

where Y_k is the local mass fraction of species k, D_k the molecular diffusion coefficient, and σ is the turbulent Schmidt number ($\sigma = 0.7$). The last term at right-hand side of Eq. (7) is mass source from reactions.

2.6. Single char combustion model

Chemical reaction kinetics for char combustion may be expressed as [28–33]:

$$2\left(\frac{\alpha+1}{\alpha+2}\right)C + O_2 \rightarrow \left(\frac{2\alpha}{\alpha+2}\right)CO + \frac{2}{\alpha+2}CO_2 \quad (A)$$

$$C + CO_2 \rightarrow 2CO \quad (B)$$

where the parameter α is the primary product ratio of CO/CO_2 given as [34]:

$$\alpha = 750 \exp\left(\frac{-7200}{T_p}\right) \quad (8)$$

The product CO leaving the particle surface is oxidized to produce CO_2 in the gas phase. This homogenous reaction is assumed as following:

$$CO + \tfrac{1}{2}O_2 \rightarrow CO_2 \quad (C)$$

To account for dissociation of CO_2 at high temperatures, a reverse reaction was considered as follows:

$$2CO_2 \rightarrow 2CO + O_2 \quad (D)$$

The complex chemistry of both formation and destruction of NO and N_2O is not completely understood. The heterogeneous reactions of char with CO, CO_2, NO, and N_2O, and the homogeneous reactions involving CO, O_2, NO, and N_2O components are therefore simplified. The char bound to nitrogen is first oxidized to NO by a reaction which is first order with respect to oxygen concentration [35]:

$$[C\text{–}N] + O_2 \rightarrow NO + [C\text{–}O] \quad (E)$$

NO reacts further with the bound nitrogen to produce N_2O according to the following heterogeneous reaction [36]:

$$[C\text{–}N] + NO \rightarrow N_2O + C \quad (F)$$

Several mechanisms have been proposed for the reduction of NO on the surface of char [35,37]. These mechanisms result in the release of N_2 and of chemisorbed oxygen as CO:

$$NO + C \rightarrow \tfrac{1}{2}N_2 + CO \quad (G)$$

The presence of CO in the gas phase enhances the rate of NO reduction. This may occur through the reaction of CO with surface-bound oxygen atoms, leading to the regeneration of surface sites for reaction with NO [37]. This reaction can be written as:

$$NO + CO \rightarrow \tfrac{1}{2}N_2 + CO_2 \quad (H)$$

N_2O reacts with char to form N_2 and a carbon–oxygen bond. Then, this bound can react with N_2O to form N_2 and CO_2. Alternatively, the chemisorbed O_2 may be released as CO [38]. In present model, the following global reaction was adopted:

$$N_2O + C \rightarrow N_2 + CO \quad (I)$$

The thermal decomposition of N_2O is expressed as:

$$N_2O \rightarrow N_2 + \tfrac{1}{2}O_2 \quad (J)$$

According to Allen et al. [39], the homogeneous destruction of N_2O in a fluidized bed combustor can occur through reactions involving: (1) H and OH radicals; (2) oxygen radicals; and (3) CO in the presence of water. The overall reaction is written as:

$$N_2O + CO \rightarrow N_2 + CO_2 \quad (K)$$

Table 1
Reactions used in the model

Reaction	Catalyst	Reaction rate (mol/m^3 s)	Kinetic constant (s^{-1})	Reference
(A)	Heterogeneous	$R_A = k_A Y_{O_2}$	$k_A = 11.26 \times 10^5 T_p \exp(-1.8 \times 10^5/RT_p)$	Field [42]
(B)	Homogeneous	$R_B = k_B Y_{CO_2}$	$k_B = 5.33 \times 10^6\ T_p \exp(-2.28 \times 10^6/RT_p)$	Solomon et al. [43]
(C)	Homogeneous	$R_C = k_C Y_{CO}$	$k_C = 2.5 \times 10^{12}\ [H_2O]^{0.5}[O_2]^{0.5} \exp(-1.995 \times 10^5/RT_g)$	Hautman et al. [44]
(D)	Homogeneous	$R_D = k_D Y_{CO_2}$	$k_D = 7.5 \times 10^{11} \exp(-46500/T_g)$	Cooper and Hallett [33]
(E)	Char	$R_E = k_E Y_{O_2}$	$k_E = (2(\alpha+1)/\alpha+2)k_A$	De Soete et al. [35]
(F)	Char	$R_F = k_F Y_{NO}$	$k_F = 15.0 \times 10^6 \exp(-9000/T_p)$	De Soete et al. [35]
(G)	Char	$R_G = k_G Y_{NO}$	$k_G = 2778 \times 10^6 \exp(-14193/T_p)$	De Soete et al. [35]
(H)	Char	$R_H = k_H Y_{NO}$	$k_H = 5.67 \times 10^3 T_g \exp(-13952/T_g)$	Chan et al. [37]
(I)	Homogeneous	$R_I = k_I Y_{N_2O}$	$k_I = 66.8 \times 10^6 \exp(-16677/T_p)$	Chan et al. [37]
(J)	Homogeneous	$R_J = k_J Y_{N_2O}$	$k_J = 1.75 \times 10^8 \exp(-23800/T_g)$	Bonn et al. [45]
(K)	Char	$R_k = k_k Y_{N_2O}$	$k_k = 2.51 \times 10^8 Y_{CO} \exp(-23180/T_g)$	Allen et al. [39]

The reaction rates of these heterogeneous and homogeneous reactions are summarized in Table 1.

2.7. Boundary conditions and simulation procedures

The inlet gas compositions, temperature and velocity were specified. At the outlet, the continuous gas flow boundary condition was used. No-slip boundary conditions for gas flow at the particle surface and walls are applied:

$$u = k = \varepsilon = 0 \tag{9}$$

The boundary condition for gas species at the particle surface is:

$$\left(\rho_k D_k + \frac{\mu_g}{\sigma}\right) \left.\frac{\partial Y_k}{\partial x_j}\right|_R - \dot{m}_d Y_{k,R} = R_k \tag{10}$$

where $\dot{m}_d$ is the total mass production rate from char combustion. The boundary condition of temperature at both particle and wall surfaces is:

$$\left.\frac{\partial T}{\partial x_j}\right|_R = 0 \tag{11}$$

The governing Eqs. (1)–(7) and gas species mass fractions coupling with reaction kinetics were solved using the finite volume methods [40] with appropriate boundary conditions. The porous structure of a cluster of particles was assumed with a specified porosity of the cluster in present simulations, shown in Fig. 1. The parameters used in the simulations are listed in Table 2. The physical domain of cylindrical boundary of each particle is mapped onto a square domain in the computation domain using the body-fitted coordinate to make the grids fit the boundary of particles [41]. Nineteen char particles form the cluster and give a cluster porosity of 0.8. Fresh gas flow into the cluster, reacted with char particles there, and product gases out of the cluster. These char particles are assumed to stationary while combusted. A set of simulation needs about 24 h of CPU time to reach the convergence on a PC (80 GB hard disk, 128 Mb Ram and of 600 MHz CPU).

3. Simulation and analysis

3.1. Base case simulation

In this simulation, the inlet gas velocity, temperature, and porosity were set to be 5.0 m/s, 1400 K, and 0.8, respectively, except otherwise specified.

Fig. 2 shows the axial velocity profiles of gas at the various positions. A small amount of gas flows through the cluster, while most gas bypasses it because of resistance of the cluster. There is less flow or somewhat back flow behind the cluster. In reality

Table 2
Parameters used in the simulations

Parameter	Value	Parameter	Value
Inlet gas velocity	1.5 m/s, 5.0 m/s	Diameter of particle	75 μm
Inlet gas temperature	1400 K	Density of particle	1600 kg/m^3
Inlet concentration of oxygen	0.23	Temperature of particle	1400 K
Inlet concentration of moisture	0.05	Radius of cluster, R_c	365 μm
Activation energy in Reaction (A)	1.8×10^5 J/mol	Pre-exponential factor in Reaction (A)	11.26×10^5
Diffusion coefficient of O_2	0.20 cm^2/s	Diffusion coefficient of H_2O	0.2178 cm^2/s
Diffusion coefficient of CO_2	0.1381 cm^2/s	Diffusion coefficient of N_2O	0.1436 cm^2/s
Diffusion coefficient of CO	0.1801 cm^2/s	Diffusion coefficient of NO	0.1729 cm^2/s
Empirically determined constant, C_1	1.44	Empirically determined constant, C_2	1.92
Empirically determined constant, C_μ	0.09	Empirically determined constant, σ_k	1.0
Empirically determined constant, σ_ε	1.3	Empirically determined constant, σ_h	1.0
Length of computing zone	20 mm	Width of computing zone	7.5 mm
Distance from inlet to cluster center	4.0 mm	Particle number in cluster	19
Cluster porosity	0.8	Cell number ($n_r \times n_x$)	195 × 320

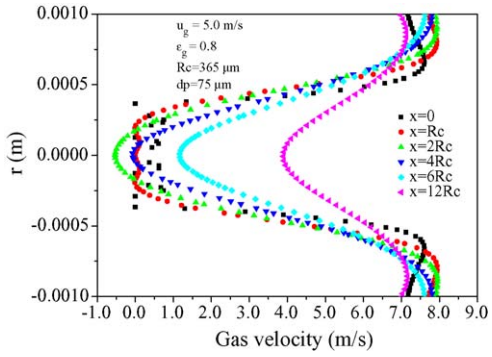

Fig. 2. Profile of gas velocity in the cluster.

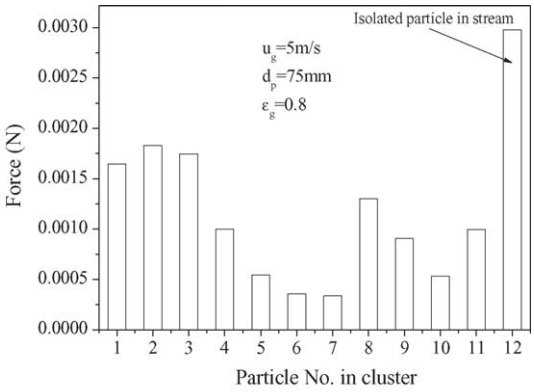

Fig. 4. Profile of forces acting on each particle in the cluster and an isolated particle in stream.

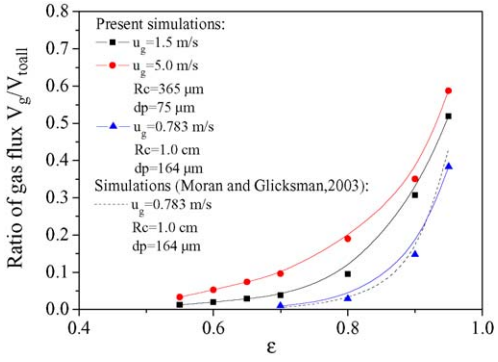

Fig. 3. Ratio of gas flux through cluster to total gas flux as a function of porosity.

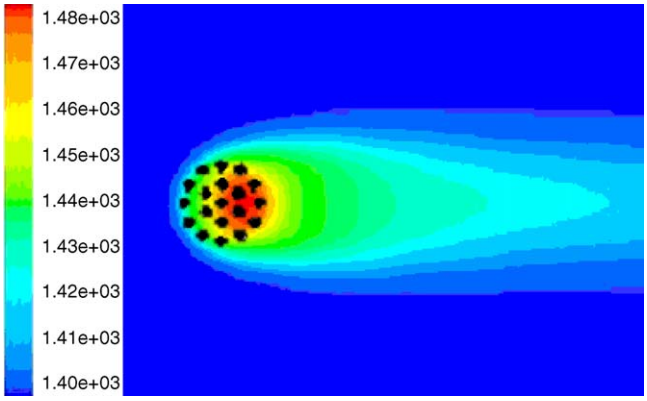

Fig. 5. Distribution of gas temperature.

the cluster may deform and should have intensive effects on gas flow in the wake region.

Ratios of gas flux through the cluster to inlet gas flux as a function of porosity are shown in Fig. 3. Three respective inlet velocities of 0.783, 1.5 and 5.0 m/s are modeled and shown in this figure. Simulated results by Moran and Glicksman [19] were given by means of Adina-F CFD program. As the porosity approaches to zero, the gas flux passing through the cluster goes to zero since the cluster becomes a solid disk. With the increase of porosity, the ratio of gas flux is increased. As the porosity goes to one, the ratio of gas flux will approach to one. From this figure we see that at the porosity of about 80–90% the ratio of gas flux passing through the cluster is exponentially increased. We see that the gas flux through the cluster increases with increase of inlet gas velocity. It is expected that when the gas velocity increases to certain value, the cluster will breakup.

The forces acting on each particle are the summation of pressure and viscous forces. Fig. 4 shows the force acting on each particle in the cluster. Each particle in the cluster is subject of different forces acting on it. The highest forces are those facing the stream and the lowest are those located at the backside of cluster. The variations of forces on particles are about four times of difference. The force acting on an isolated particle in the stream is also given in Fig. 4. We found that force on an isolated

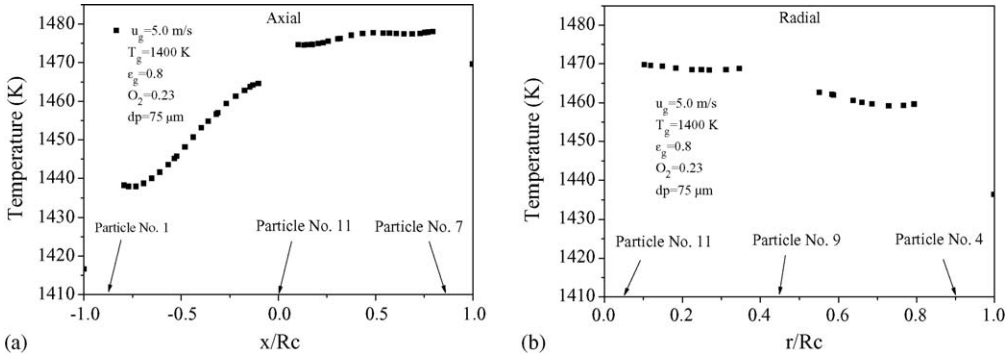

Fig. 6. Distributions of gas temperature along axial and radial directions in a cluster: (a) axial and (b) radial.

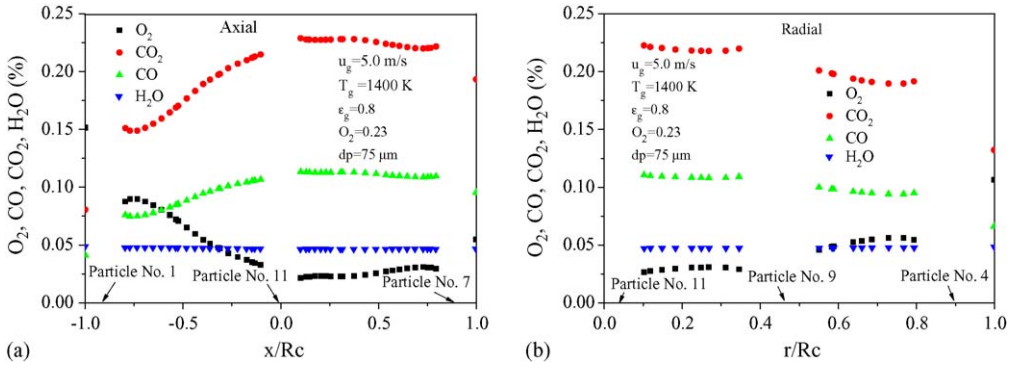

Fig. 7. Concentration distributions of gas species along axial and radial directions in a cluster: (a) axial and (b) radial.

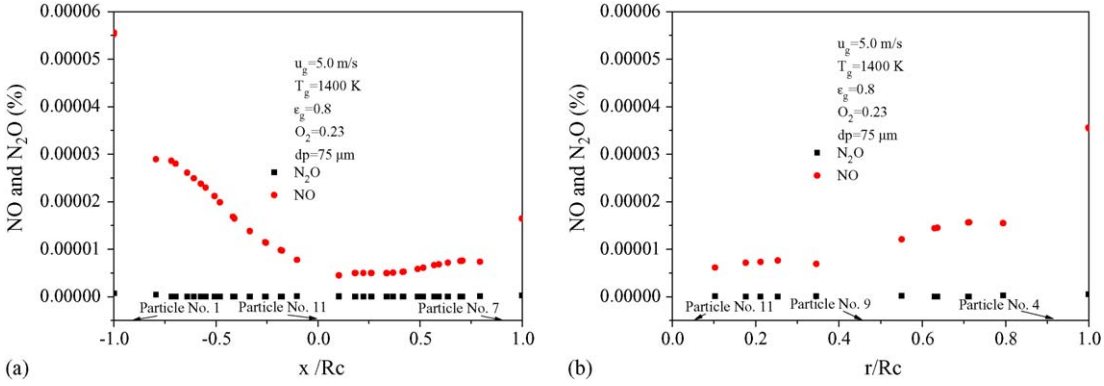

Fig. 8. Concentration distributions of NO and N_2O species along axial and radial directions in a cluster.

particle is much larger than that of particles with a cluster due to the relatively low kinetic energy received by particles with a cluster.

Fig. 5 shows the temperature distribution. The hot spot is found at the backside of cluster. As expected, the relatively higher temperatures are in the cluster and downstream of the cluster due to exothermic combustion. Figs. 6a and b shows the temperature profiles in axial and radial directions, respectively. Similar to temperature distribution shown in Fig. 5, in axial direction, the particles faced the incoming gas stream are cooled down by relatively lower temperature gas flow and the gas temperature is then raised by the char combustion at the backside of the cluster. Due to convective heat transfer, gas temperatures near the outside of the cluster are lower than those inside the center of the cluster, as shown in Fig. 6b.

Fig. 7a and b shows, respectively, the axial and radial distributions of gas species across the center of the cluster. The O_2 concentration decreases while CO_2 concentration increases along flow direction. Char combustion consume O_2 and increases both CO and CO_2 concentrations in the cluster. Fig. 8a and b shows the distribution of NO and N_2O species in the cluster. The NO concentration decreases along flow direction but increases in the radial direction. The NO concentration changes in both axial and radial directions but N_2O is hardly found in the cluster because of N_2O reacted with CO to produce nitrogen and carbon dioxide (Reaction (K)). The local minimum concentration of NO is

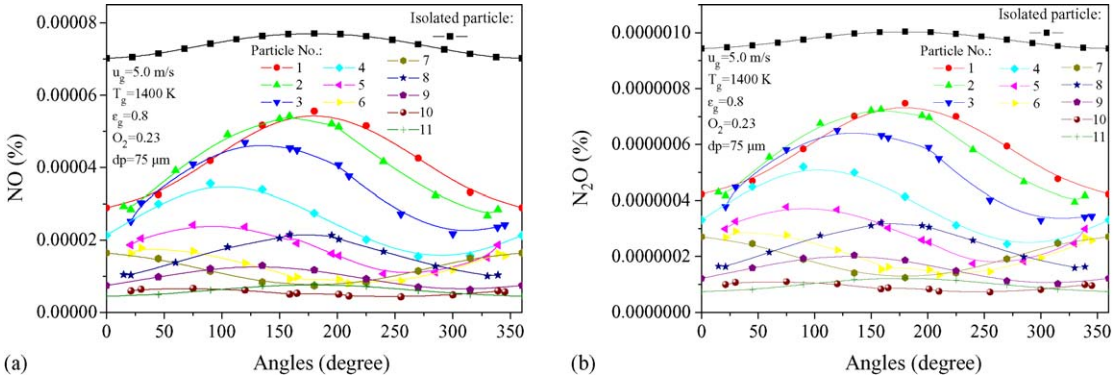

Fig. 9. (a and b) Concentration distributions of NO and N_2O species of each particle in a cluster and an isolated particle in stream.

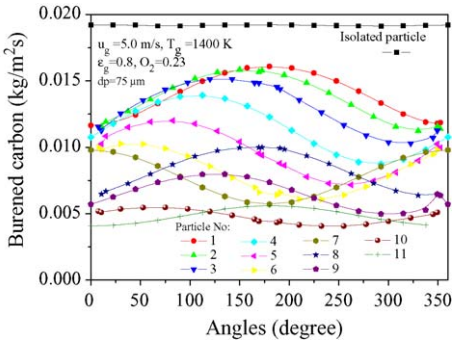

Fig. 10. Carbon burnout of each particle in a cluster and an isolated particle.

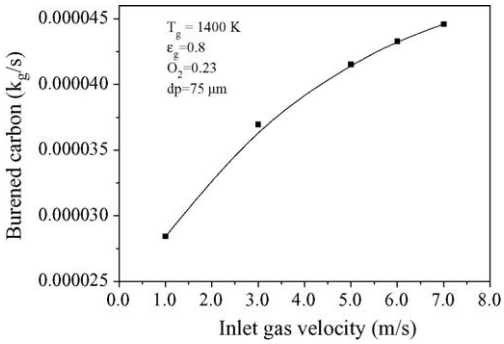

Fig. 12. Computed carbon burnout as a function of inlet gas velocity.

pretty low in the center of the cluster. Compared NO and N_2O concentration around surfaces of each particle in the cluster and with those in isolated particle, formations of NO and N_2O are significantly reduced, as shown in Fig. 9, in which 0° indicating the gas axial flow direction while 180° against the axial flow direction. Refer to orientation angle of the particles sketched in Fig. 1.

Variations reactions on a particle surface are clearly displayed in Fig. 10. Carbon burnout for each particle in the cluster as well as an isolated particle is shown. Combustion rates are affected by orientation of particles in a cluster but not by orientation of an isolated particle. Fig. 11 shows the consumed carbon as a function of specified cluster porosity. With increase of porosity, the more gas passes through the cluster and increases the combustion rate, hence the carbon of cluster is consumed.

3.2. Effect of inlet gas velocity

With introducing more gas to the riser, more "fresh" oxygen is provided to oxidize the char particles. Fig. 12 indicates that carbon burnout increases with increase of inlet gas velocity for inlet gas velocities in the ranges of 1–7 m/s. However, only sufficient oxygen concentration is required to burn the char particles. As shown in the figure, the burnout curve tends to be flat with further increasing inlet gas velocity.

3.3. Effect of inlet gas temperature

Exothermic reactions, such as char combustion, favor high temperature. As shown in Reaction (A) in Table 1 and Eq. (8), char combustion increases with increasing temperature. Fig. 13 shows the carbon burnout of particles in the cluster as a function of inlet gas temperature. The inlet gas temperature affects exponentially carbon burnout of char particles in the cluster.

3.4. Effect of activation energy of char particles in heterogeneous reaction

The reactivity of carbon particles is characterized by the activation energy and a pre-exponential factor via the Arrhenius equation. Thermal analyses suggest that the activation energy is the predominant factor in the reactivity equation [46]. Activation energy, essentially, affects the temperature sensitivity of the reaction rate, whereas the pre-exponential factor is related more to material structure. Char reactivity, therefore, may be sufficiently characterized by its activation energy value alone. Fig. 14 shows axial profile of gas temperature as a function of activation energy as in the form of Reaction (A). The gas temperature decreases with increase of the activation energy due to more reaction energy required for combustion and less heat generated from combustion. At activation energy equal to 3.6×10^8 J/mol, no combustion can occur and therefore gas temperature is almost constant same as the inlet temperature. Similarly, activation energy affects combustion and hence oxygen consumption (shown in Fig. 15) and burnout (Fig. 16) which burnout drops dramatically with increase of activation energy.

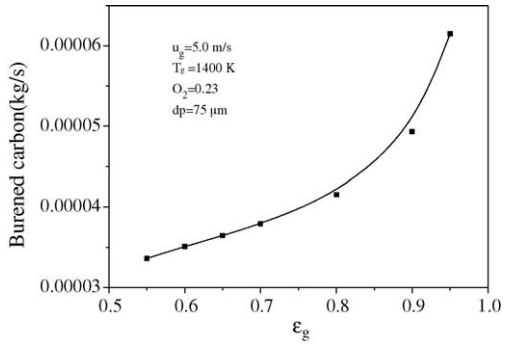

Fig. 11. Carbon burnout of cluster as a function of porosity.

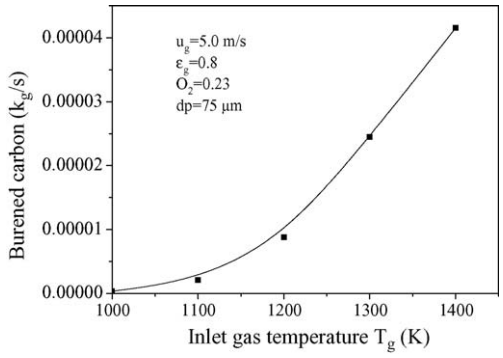

Fig. 13. Computed carbon burnout as a function of inlet gas temperature.

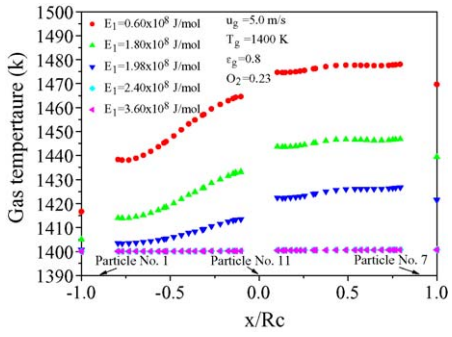

Fig. 14. Profile of gas temperature in a cluster.

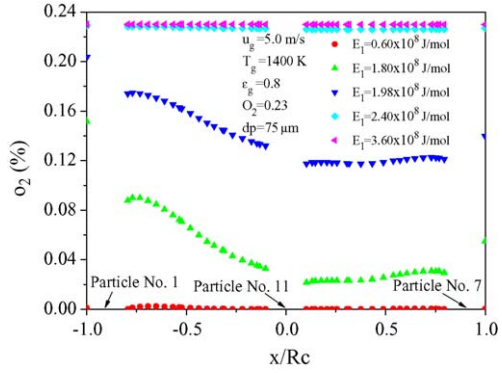

Fig. 15. Profile of oxygen concentration in a cluster.

3.5. Effect of inlet concentration of oxygen

Fig. 17 shows carbon burnout of the cluster, averaged from all particles, as a function of inlet concentration of oxygen with inlet gas velocity and porosity of 5.0 m/s and 0.8, respectively. The oxygen specified at inlet is from 0.08 to 0.23 mol%. With the increase of the inlet concentration of oxygen, burnout increases. The inlet oxygen concentration affects significantly the carbon consumption.

3.6. Effect of particle distribution in a cluster

Particles in a cluster should change from time to time, location in a riser, and dependent on environmental fluidizing conditions. To estimate the effects of particle distribution in a cluster, two cases are simulated. One is that all particles in a cluster are shifted 10° counter-clock wise from base case (Fig. 1), the second case is that all particles in a cluster are shifted 20° counter-clock wise from base case. These two cases are shown in Fig. 18a and b, respectively. Effects of the redistributed particles in clusters change gas flow route through clusters and resulted in force acting on particles and surface combustion rate. Figs. 19 and 20 depict these effects. Although, redistribution of particles in clusters increases slightly gas flux, total force acting on particles, and burnout, such effects are small enough to be negligible. The data show that the ratio of gas flux change is less than 3.0%, increment of total force on particles is less than 0.2%, and burnout variation is less than 0.7%.

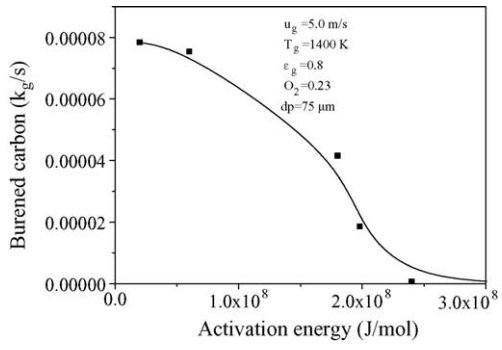

Fig. 16. Distribution of carbon burnout as a function of activation energy.

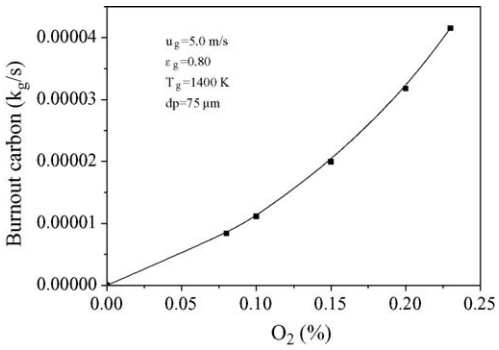

Fig. 17. Distribution of carbon burnout of a cluster vs. inlet oxygen concentration.

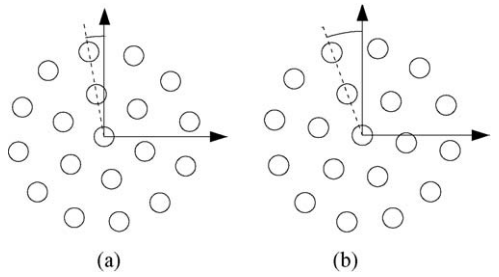

Fig. 18. (a and b) Distributions of particles in cluster.

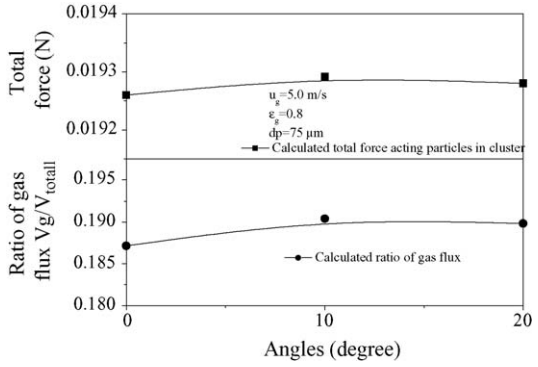

Fig. 19. Effects of distribution particles in cluster on gas flux ratio and total force.

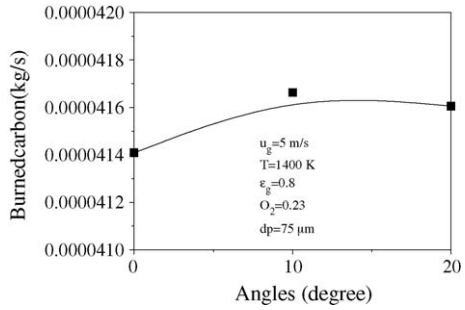

Fig. 20. Effect of distribution particles in cluster on carbon burnout.

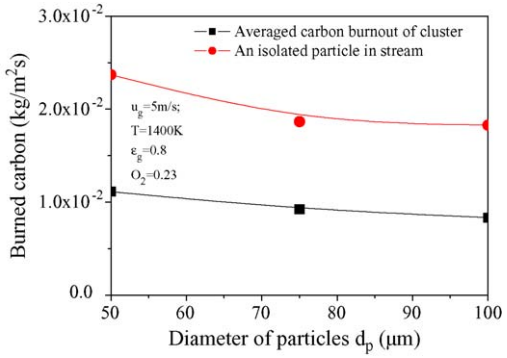

Fig. 21. Profile of carbon burnout as a function of particle diameter.

3.7. *Effect of particle size*

Fig. 21 shows various particle diameter effects on carbon burnout for particles in a cluster and an isolated particle in the riser. Particle surface area increases with square of particle diameter and therefore increases surface combustion of char particles. As expected, computed carbon burnout decreases with increase of particles diameter. From particle diameter increasing from 50 to 100 μm, the burnout decreases about 25–30% for both cluster and isolated particle cases. The average carbon burnout for each particle in the cluster is about four times less than that for an isolated particle, mainly due to relatively lower gas flow around the particles in the cluster than gas flow around the isolated particle.

4. Conclusions

A numerical model was constructed to study the behaviors of flow and combustion of char particle cluster in a CFB riser. The gas flow passing through clusters, gas temperature, gas species variations, and carbon burnout in the cluster were predicted. The carbon burnout of particles in the cluster is lower than that of the isolated particle under the fluidization conditions. Carbon burnout increases with increase of cluster porosity. Burnout of char particles with a cluster is less than that of isolated char particles in the stream. Formation of NO and N_2O are restrained from particle clustering.

Actually, a riser as well as structure of a cluster is three-dimensional, particles are somewhat randomly positioned in the cluster. A cluster is not quiescent and its size and shape are changing from time to time and dependent on fluidizing condition. Detailed modeling and analysis of two-phase gas–particle reacting flow with char particle combustion in CFB riser are required and will be further pursued.

Acknowledgement

This work was supported by the National Science Foundation in China through Grant No. 50376013, and the cooperative project by NSFC-Petro China Company Limited under Grant No. 20490200.

References

[1] P. Basu, Combustion of coal in circulating fluidized-bed boilers: a review, Chem. Eng. Sci. 54 (1999) 5547–5557.
[2] E.J. Anthony, Fluidized bed combustion of alternative solid fuels: status, successes and problems of the technology, Prog. Energy Combust. Sci. 21 (1995) 239–268.
[3] L. Reh, Challenges of circulating fluid-bed reactors in energy and raw materials industries, Chem. Eng. Sci. 54 (1999) 5359–5368.
[4] H. Johnsson, F. Johnsson, Measurements of local solids volume-fraction in fluidized bed boilers, Powder Technol. 115 (2001) 13–26.
[5] T. Knobig, J. Werther, L.E. Amand, B. Leckner, Comparison of large- and small-scale circulating fluidized bed combustors with respect to pollutant formation and reduction for different fuels, Fuel 77 (1998) 1635–1642.
[6] J. Yerushalmi, N.T. Cankurt, D. Geldart, B. Liss, Flow regimes in vertical gas–solid contact systems, AIChE Symp. Ser. 74 (1978) 1–13.
[7] C.J. Chen, Experiments that address phenomenological issues in fast fluidization, Chem. Eng. Sci. 54 (1999) 5529–5539.
[8] M. Horio, H. Kuroki, Three-dimensional flow visualization of dilutely dispersed solids in bubbling and circulating fluidized beds, Chem. Eng. Sci. 49 (1994) 2413–2421.
[9] C.H. Soong, K. Tuzla, J.C. Chen, in: J.F. Large, C. Laguerie (Eds.), Experimental Determination of Clusters Size and Velocity in Circulating Fluidized Beds, Fluidization VIII Engineering Foundation, New York, 1995, pp. 219–227.
[10] V.D. Moortel, E. Azario, R. Santini, L. Tadrist, Experimental analysis of the gas–particle flow in a circulating fluidized bed using a phase Doppler particle analyzer, Chem. Eng. Sci. 53 (1998) 1883–1899.
[11] A.K. Sharma, K. Tuzla, J. Matsen, J.C. Chen, Parametric effects of particle size and gas velocity on cluster characteristics in fast fluidized beds, Powder Technol. 111 (2000) 114–122.
[12] S.V. Manyele, J.H. Parssinen, J.X. Zhu, Characterizing particle aggregates in a high-density and high-flux CFB riser, Chem. Eng. J. 88 (2002) 151–161.
[13] N. Mostoufi, J. Chaouki, Flow structure of the solids in gas–solid fluidized beds, Chem. Eng. Sci. 59 (2004) 4217–4227.
[14] P.D. Noymer, L.R. Glicksman, Cluster motion and particle-convective heat transfer at the wall of a circulating fluidized bed, Int. J. Heat Mass Transfer 41 (1998) 147–158.
[15] T.J. O'Brien, M. Syamlal, Fossil fuel circulating fluidized bed, AIChE Symp. Ser. 87 (1991) 127–136.
[16] Y. Tsuji, T. Tanaka, S. Yonemura, Cluster patterns in circulating fluidized beds predicted by numerical simulation (discrete particle model versus two-fluid model), Powder Technol. 95 (1998) 254–264.
[17] E. Helland, R. Occelli, L. Tadrist, Numerical study of cluster formation in a gas–particle circulating fluidized bed, Powder Technol. 110 (2000) 210–221.
[18] D.Z. Zhang, W.B. VanderHeyden, The effects of mesoscale structures on the macroscopic momentum equations for two-phase flows, Int. J. Multiphase Flow 28 (2002) 805–822.
[19] J.C. Moran, L.R. Glicksman, Experimental and numerical studies on the gas flow surrounding a single cluster applied to a circulating fluidized bed, Chem. Eng. Sci. 58 (2003) 1879–1886.

[20] R. Sotudeh-Gharebaagh, R. Legros, J. Chaouki, L. Paris, Simulation of circulating fluidized bed reactors using ASPEN PLUS, Fuel 77 (1998) 327–337.
[21] C.K. Park, P. Basu, A model for prediction of transient response to the change of fuel rate to a circulating fluidized bed boiler furnace, Chem. Eng. Sci. 52 (1997) 3499–3509.
[22] X.S. Wang, B.M. Gibbs, M.J. Rhodes, Modelling of circulating fluidized bed combustion of coal, Fuel 73 (1994) 1120–1129.
[23] J. Adanez, P. Gayan, G. Grasa, L.F. de Diego, L. Armesto, A. Cababillas, Circulating fluidized bed combustion in the turbulent regime: modeling of carbon combustion efficiency and sulphur retention, Fuel 80 (2001) 1405–1414.
[24] K. Myohanen, T. Hyppanen, J. Miettnen, R. Parkkonen, Three-dimensional modeling and model validation of circulating fluidized bed combustion, in: Proceedings of the 17th International Conference on Fluidized Bed Combustion, 2003, pp. 293–303.
[25] J. Knoebig, K. Luecke, J. Werther, Mixing and reaction in the circulating fluidized bed—a three-dimensional combustor model, Chem. Eng. Sci. 54 (1999) 2151–2160.
[26] L.D. Smoot, P.J. Smith, Coal Combustion and Gasification, Plenum Press, New York, 1985.
[27] I. Glassman, Combustion, Academic Press, New York, 1987.
[28] J.B. Howard, G.C. Williams, D.H. Fine, Kinetics of carbon monoxide oxidation in postflame gases, in: 14th Symposium (International) on Combustion, 1973, pp. 975–986.
[29] C.K. Westbrook, F.L. Dryer, Chemical kinetic modeling of hydrocarbon combustion, Prog. Energy Combust. Sci. 10 (1984) 1–57.
[30] M.L. Hobbs, P.T. Radulovic, L.D. Smoot, Modelling fixed-bed coal gasifier, AIChE J. 38 (1992) 681–702.
[31] J. Ding, Analysis of hydrodynamics and chemical reactions in circulating fluidized beds, in: M. Kwauk, J. Li (Eds.), Circulating Fluidized Beds, vol. V, 1996, pp. 446–451.
[32] S. Kulasekaran, T.M. Linjewile, K. Pradeep, P.K. Agarwal, Mathematical modeling of fluidized bed combustion: simultaneous combustion of char and combustible gases, Fuel 78 (1999) 403–417.
[33] J. Cooper, W.L.H. Hallett, A numerical model for packed-bed combustion of char particles, Chem. Eng. Sci. 55 (2000) 4451–4460.
[34] R.R. Rajan, C.Y. Wen, A comprehensive model for fluidized bed coal combustors, AIChE J. 26 (1980) 642–655.
[35] G.G. De Soete, E. Croiset, J.R. Richard, Heterogeneous formation of nitrous oxide from char bound nitrogen, Combust. Flame 117 (1999) 140–154.
[36] G.F. Krammer, A.F. Sarofim, Reaction of char nitrogen during fluidized bed coal combustion—influence of nitric oxide and oxygen on nitrous oxide, Combust. Flame 97 (1994) 118–124.
[37] L.K. Chan, A.F. Sarofim, J.M. Beer, Kinetics of NO–carbon reaction at fluidized bed combustion conditions, Combust. Flame 52 (1983) 37–44.
[38] L.E. Amand, S. Andersson, Emissions of nitrous oxide (N_2O) from fluidized bed boilers, in: Proceedings of the 10th International Conference on Fluidized Bed Combustion: ASME, 1989, pp. 49–55.
[39] M.T. Allen, R.A. Yetter, F.L. Dryer, High pressure studies of moist carbon monoxide/nitrous oxide kinetics, Combust. Flame 108 (1997) 449–470.
[40] S.V. Patankar, Numerical Heat Transfer and Fluid Flow, McGraw-Hill, New York, 1998.
[41] H. Yurong, L. Huilin, S. Qiaoqun, Y. Lidan, Z. Yunhua, D. Gidaspow, J. Bouillard, Hydrodynamics of gas–solid flow around immersed tubes in bubbling fluidized beds, Powder Technol. 145 (2004) 88–105.
[42] M.A. Field, Rate of combustion of size-graded fractions of char from a low-rank coal between 1200 K and 2000 K, Combust. Flame 13 (1969) 237–252.
[43] P.R. Solomon, T.H. Fletcher, R.J. Pugmire, Progress in coal pyrolysis, Fuel 72 (1983) 587–596.
[44] D.J. Hautman, F.L. Dryer, K.P. Schug, I. Glassman, A multiple-step over kinetic mechanism for the oxidation of hydrocarbons, Combust. Sci. Technol. 25 (1981) 219–232.
[45] B. Bonn, G. Pelz, H. Baumann, Formation and decomposition of N_2O in fluidized bed boilers, Fuel 74 (1995) 165–171.
[46] R. Hurt, J. Sun, M. Lunden, A kinetic model of carbon burnout in pulverized coal combustion, Combust. Flame 113 (1998) 181–197.